CrossMark

RESEARCH PAPER

Breakup of confined drops against a micro-obstacle: an analytical model for the drop size distribution

Akio Nishimura[1] · Alexandre Schmit[2] · Louis Salkin[3] · Laurent Courbin[3] · Pascal Panizza[3]

Abstract A confined drop flowing against a rectangular obstacle placed off-center in a microfluidic conduct may break into two daughter droplets of different volumes when the capillary number at play $\mathcal{C}$, the ratio between viscous and capillary effects, exceeds a threshold $\mathcal{C}_b$. We study the influence of the viscosity ratio p between dispersed and continuous phases on that process by discussing the experimental variations of the volume fraction of the daughter droplets with $\mathcal{C}$ and p. A single free parameter model that yields an analytical formula for the volume of the daughter droplets as a function of the variables at play is introduced. Using this model that well describes our experiments, we accurately determine $\mathcal{C}_b$ for different p. Our findings underline the key role of confinement on drop breakup showing that $\mathcal{C}_b$ is three orders of magnitude smaller than the value found in bulk experiments under shear flow and that $\mathcal{C}_b$ decreases with p in our study.

Keywords Two-phase flows · Droplets · Emulsions · Confined flows

✉ Pascal Panizza
pascal.panizza@univ-rennes1.fr

Laurent Courbin
laurent.courbin@univ-rennes1.fr

[1] United Graduate School of Agricultural Science, Tokyo University of Agriculture and Technology, 358 Saiwaicho, Fuchu shi, Tokyo 1838509, Japan

[2] NANO, UR1268, BIA, INRA, rue de la Géraudière, 44316 Nantes, France

[3] Institut de Physique de Rennes (IPR), UMR CNRS 6251, Université Rennes 1, 35042 Rennes, France

1 Introduction

Emulsions, i.e., metastable dispersions of two immiscible liquids, are used in a variety of industrial, engineering and biomedical applications (Leal-Calderon et al. 2007). Examples include end products in the cosmetic and food industries, dynamical templates for the production of colloidal suspensions, capsules or liposomes in material science and microreactors in high-throughput biomicrofluidic assays. All of these applications require to control the drop size distribution as the physical properties of these materials are highly size dependent. Hence, drop breakup is a central topic in emulsion science. For any drop breakup experiment, the key issues are to identify the experimental conditions for breaking a mother drop and to predict the size of the daughter droplets as a function of the parameters at play.

Since the pioneering studies of the deformation and rupture of an isolated drop in bulk by Taylor (1932, 1934), the topic has been widely studied for many flow configurations such as linear two-dimensional flows (Bentley and Leal 1986), simple shear flows (Janssen and Meijer 1993) and extensional flows (Stone 1994). For low Reynolds numbers and Newtonian fluids, it is known that drop breakup is mainly controlled by two dimensionless parameters: the capillary number $\mathcal{C}$ defined as the ratio between viscous and capillary forces and p the viscosity ratio between dispersed and continuous phases. Drop breakup usually occurs when the capillary number exceeds a threshold $\mathcal{C}_b$ that varies with p and the nature of the flow (Grace 1982). Under shear flow, for instance, an isolated droplet adopts an ellipsoidal shape when $\mathcal{C} < \mathcal{C}_b$. At $\mathcal{C}_b$, the droplet draw ratio, defined as the drop length needed for breakup over the original droplet diameter, is a non-monotonic function of p: it is either decreasing

($p < 10^{-1}$) or increasing ($p > 10^{-1}$) with p (Grace 1982). At either very small ($p < 10^{-5}$) or very large ($p > 3$) viscosity ratios, the droplet draw ratio approaches one hundred, a breaking drop is then a very long thread that breaks because of the growth of a capillary-wave instability (Rayleigh 1878), or other processes, e.g., tip streaming (Torza et al. 1972; Grace 1982) or end pinching (Stone and Leal 1989). In all cases, smaller droplets with a broad size distribution are produced. Around $p = 10^{-1}$, the droplet draw ratio is minimum and the size of a drop at breakup is only a few times the original one. This drop then breaks into smaller ones having a narrow size distribution centered around a mean size $\sim \mathcal{C}^{-1}$. When $p > 4$, the droplet deformation remains small and breakup is never observed. These results strongly depend on the rheological properties of the two-phase fluid. For instance, for fluids having a viscoelastic component, breakup can occur in shear flows when $p > 4$ (Mighri et al. 1998). Also, when shearing alters the microstructure of the two-phase fluid, the response of sheared drops may become non-stationary and sustained droplet size oscillations can be observed (Courbin et al. 2004a). For this class of fluids, the breakup of drops may even occur without elongation (Courbin et al. 2004b). In confined flows, $\mathcal{C}_b$ does not only depend on p but also on the degree of confinement. This parameter tends to increase the threshold for breakup at low viscosity ratios, whereas $\mathcal{C}_b$ decreases with the confinement at large p (Vananroye et al. 2006, 2007). For sufficiently confined sheared flows, Vananroye et al. (2006) have even shown that breakup can occur when $p > 4$. Also, Newtonian drops in viscoelastic matrix break at very small values of $\mathcal{C}_b$ in confined conditions (Cardinaels and Moldanaers 2011; Guido 2011). By contrast, in the case of viscoelastic drops, $\mathcal{C}_b$ may either increase or decrease depending on the drop viscoelasticity (Gupta and Sbragaglia 2014).

Recent advances in microfluidics for material science (Chu et al. 2007; Shah et al. 2008; Engl et al. 2008), biotechnology and chemistry (Teh et al. 2008; Trivedi et al. 2010; Seeman et al. 2012) have inspired investigations of the breakup of confined drops in various microfluidic geometries. For instance, one can actively break microfluidic drops using an electric field (Link et al. 2006) or an optical approach (Baroud et al. 2007). However, most studies exploit passive (geometry-based) methods that solely rely on the flow geometry. Examples include cross-flow microchannels (Tan et al. 2008; Cubaud 2009; Che et al. 2011), T-junctions (Link et al. 2004; de Menech 2006; Leshansky and Pismen 2009; Afkhami et al. 2011; Bedram and Moosavi 2011; Samie et al. 2013; Salkin et al. 2013; Wang and Yu 2015), Y-junctions (Ménétrier-Deremble and Tabeling 2006; Abate and Weitz 2011; Bedram et al. 2015; Zheng et al. 2016) and micro-obstacles (Link et al. 2004;

Protière et al. 2010; Chung et al. 2010; Salkin et al. 2012; Li et al. 2014). The earliest work by Link et al. (2004) has shown that breaking a drop or a bubble into two daughter droplets or bubbles of different sizes can be achieved by drop impact either against an off-centered micro-obstacle in a channel or at a T-junction, i.e., the inlet node of a loop having two arms of different lengths: other governing parameters being fixed, the volume fraction ϕ_i ($i = 1$ or 2) of the two daughter droplets or bubbles is controlled either by the distance between obstacle and axis of a channel or by the ratio of the lengths of the two arms of a loop. Similar to bulk experiments, for these two microfluidic configurations, breakup also occurs when the capillary number is larger than a threshold $\mathcal{C}_b$. Many of the works cited above combine experiments and theory to understand how $\mathcal{C}_b$ and ϕ_i vary with the geometrical, hydrodynamical and physicochemical variables at play. In particular cases, ϕ_i solely depends on the geometry and can be explained using simple physical arguments (Link et al. 2004; Salkin et al. 2013). In most cases, however, modeling experimental findings is a challenging task since the number of governing parameters is large. For drop impact against micro-obstacles, Salkin et al. (2012) have shown that the use of a rectangular obstacle allows one to establish a theoretical framework that provides a full description of the experiments. Notably, the model introduced by Salkin et al. (2012) has been successfully employed to rationalize non-trivial experimental results such as the either monotonic or non-monotonic evolution of $\mathcal{C}_b$ with a drop size depending on the sign of the viscosity contrast, that is, the difference between the viscosities of dispersed and continuous phases divided by the latter one. Salkin et al. (2013) have also used their theoretical framework to explain the variations of ϕ_i with numerical simulations, ϕ_i being in this case a complex function of the size and speed of a mother drop, p, the surface tension between liquid phases, and the geometrical variables.

Here, we investigate the volume fraction ϕ_i of the daughter droplets formed upon breakup of a mother drop against an off-centered rectangular obstacle as a function of the viscosity ratio p and capillary number $\mathcal{C}$. We present a model that provides an analytical expression for ϕ_i as a function of these controlling parameters and the geometrical variables. We find that the threshold in capillary number $\mathcal{C}_b$ decreases monotonically with $p = 0.2$–2 and its value is three orders of magnitude smaller than previous results for shear flows in bulk.

## 2 Experiments: setup, materials and methods

Our microchannels are made in poly-dimethylsiloxane (PDMS) using standard soft lithography (McDonald et al. 2000). They have a rectangular cross section with height

$h = 50\,\mu m$ and width $w = 130\,\mu m$ (see Fig. 1). We generate a periodic train made of monodisperse drops using a flow-focusing geometry (Anna et al. 2003). Two syringe pumps (PHD 2000, Harvard Apparatus) inject the dispersed (aqueous solution) and continuous (oil) phases at controlled flow rates which are adjusted independently until a steady flow of monodisperse drops with volume $\Omega = 1140$ pL is obtained. We herein refer to these flattened drops that are larger than w as "slugs." Details about the fluid system are given further in the text. Typical flow rates of dispersed and continuous phases are $q_w = 5$–$200\,\mu L/h$ and $q_o^f = 5$–$500\,\mu L/h$, respectively. The drops are then directed toward a rectangular obstacle (length $L = 500\,\mu m$ and width $30\,\mu m$) parallel to the walls of the channel and off-centered. As shown in Fig. 1, the two gaps (1) and (2) on both sides of an obstacle have different widths $w_1 = 70\,\mu m$ and $w_2 = 30\,\mu m$. A dilution module (Prat et al. 2006; Sessoms et al. 2010) allows for an additional injection of oil at constant flow rate $q_o^d = 0$–$1000\,\mu L/h$ to vary the drop velocity v while Ω is unchanged. This module is far upstream from the obstacle so that the flow is steady near the obstacle (see Fig. 1) and the distance λ between two consecutive drops is large enough to prevent drop-to-drop interactions that are

known to affect drop breakup (Belloul et al. 2011; Schmit et al. 2015).

We record videos of the flow nearby the obstacle with a high-speed camera (Phantom V7) working at 1000 frames/s for a resolution of 64×512 pixels^2. The production rate f of the drops, Ω, v, their size L_d and the sizes L_1 and L_2 of the two daughter droplets, respectively, flowing the gaps (1) and (2) are obtained from image processing using a custom-written MATLAB software. The volume of a mother drop, $\Omega = \frac{q_w}{f}$, is first determined by measuring the droplet production rate f. One then computes the effective droplet size $L_d = 220 \pm 20\,\mu m$ according to $L_d = \frac{\Omega}{hw}$. The volumes Ω_1 [gap (1)] and Ω_2 [gap (2)] of the daughter drops are deducted from the measurements of their surface areas by using the formulae predicting the volume of a confined droplet (see Fig. 2). These formulae are valid provided that the capillary number at play is sufficiently small so that the droplet shape is only set by its degree of confinement. Note that we have neglected the thickness of the lubrication films that always exist between a non-wetting droplet and the microchannel walls. Such lubrication films are expected to be much smaller than the characteristic sizes of the channels we use (Huere et al. 2015). Once the volumes mentioned above are obtained, the two daughter droplets effective lengths L_1 and L_2 are, respectively, determined using the two relationships $L_1 = \frac{\Omega_1}{w_1 h}$ and $L_2 = \frac{\Omega_2}{w_2 h}$. These effective lengths correspond to the lengths of cuboids having similar volumes to those of the considered droplets. As we will see further in the text, these quantities are useful parameters to model our experiments.

We use hexadecane (Sigma-Aldrich) for the continuous phase and solutions of glucose (0–38 wt%) in water for the dispersed phase. We add 15 g/L of a surfactant [sodium dodecyl sulfate (SDS), Sigma] in the aqueous solutions to hinder droplet coalescence. In our experiments, the Reynolds and capillary numbers are small and span the ranges 10^{-2}–10^{-1} and 10^{-3}–10^{-2}, respectively. The Reynolds number $\mathcal{R}$ and the capillary number $\mathcal{C}$ correspond to the ratios between inertial and viscous forces and between viscous and capillary forces, respectively. They are defined in our system as $\mathcal{R} = \frac{\rho_c v h}{\eta_c}$ and $\mathcal{C} = \frac{\eta_c v}{\gamma}$, ρ_c being the density of the continuous phase. We measure the viscosity of each liquid with an Anton Paar MCR 301 rheometer. Table 1 describes the properties of each water/SDS/glucose mixture with dynamic viscosity η_d, the viscosity of hexadecane being $\eta_c = 3$ mPa s. For the prepared mixtures, the interfacial tension between continuous and dispersed phases determined with pendant drop tensiometry is $\gamma = 5$–6.5 mN/m. In what follows, we investigate the variations of the volume fraction of the daughter droplet in the narrow gap (2), $\phi_2 = \Omega_2/\Omega$; the volume fraction of the drops in the large gap is simply $\phi_1 = \Omega_1/\Omega = 1 - \phi_2$.
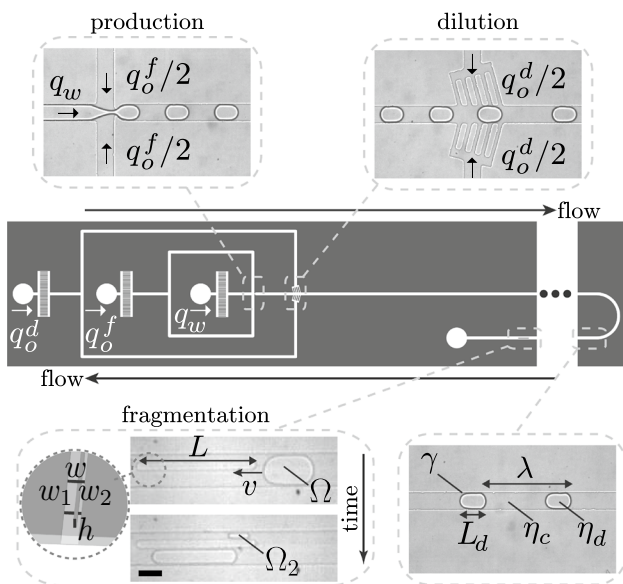
Fig. 1 *Middle panel*: Image of the photomask of the microfluidic device used in our study; defined are the flow rate of the dispersed phase q_w and the oil flow rates in the production and dilution modules, q_o^f and q_o^d, respectively. *Top panel*: Photographs showing the flow-focusing geometry that produces periodic trains of monodisperse drops and the dilution module. The *bottom panel* which consists of a photograph of the flow downstream of the dilution module and a combination of a photograph and a schematic nearby the obstacle defines the geometrical, hydrodynamical and physicochemical variables at play. *Scale bar* 100 μm

Fig. 2 This figure depicts the *shape* that a droplet seeks when it is confined in a microfluidic channel having a rectangular cross section. In this qualitative picture, the capillary number is sufficiently small so that the droplet shape only depends on its degree of confinement. Three possible cases can be obtained depending on the ratio between a drop size and channel geometry. The last column shows the surface, length and volume of a drop in these three cases

3 Experiments: results

In our experiments, we vary v while maintaining all other variables fixed. In agreement with foregoing results in the literature, when v becomes larger than threshold velocity v_b, a slug breaks in two daughter droplets when its rear edge meets the obstacle (see Fig. 1). These drops then flow in gaps (1) and (2). By contrast, when $v < v_b$, a slug does not break and flows in the larger gap. As depicted in Fig. 1, the volume Ω_2 of the droplet created in the narrow gap is smaller that that of the drop formed in gap (1). Figure 3 shows that Ω_2 is an increasing function of $v > v_b$ and that it increases with η_d for a given speed.

4 Discussion and model

We now discuss the variations of ϕ_2 with the dimensionless parameters controlling the problem, $\mathcal{C} = \frac{\eta_c v}{\gamma}$ and $p = \frac{\eta_d}{\eta_c}$. We will rationalize our findings with a theoretical framework recently introduced to describe the breakup dynamics of drops impacting a micro-obstacle (Salkin et al. 2012 and Schmit et al. 2015). We describe below the basic elements of this framework.

We assume that the speed v of a slug flowing in a channel of constant cross section $S = hw$ varies as q / S with $q = q_w + q_o^f + q_o^d$ the total flow rate. We consider that the flows of the slug and the continuous phase satisfy Darcy's law, with an effective viscosity η_d^s for the slug. η_d^s is a free parameter that accounts for viscous dissipation inside the slug, in the thin lubrication films of oil between the slug and the channel walls and in the corners of the rectangular geometry. Thus, the pressure drop Δp over a portion ℓ of the slug reads

Table 1 Composition and viscosities of the water/SDS/glucose mixtures used in our study

Amount of glucose (wt%)	Viscosity η_d (mPa s)	Symbols used in the figures
0	1	Circles
14	2.1	Squares
22	2.7	Up-pointing triangles
30	3.5	Down-pointing triangles
34	4.1	Diamonds
38	5.2	Times sign

$$\Delta p_{visc} = \frac{\eta_d^s \ell q}{h^3 w} f\left(\frac{w}{h}\right), \tag{1}$$
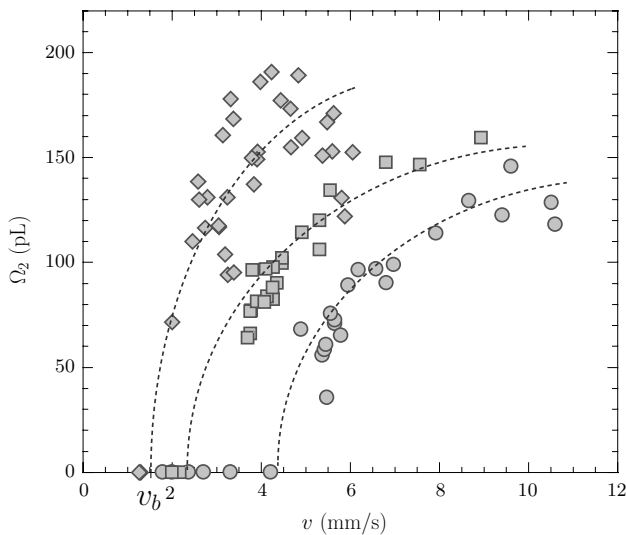
with

$$f(x) = \frac{\pi^2}{4x^2}\left[\sum_{j=1}^{\infty}\sum_{k=1}^{\infty}\frac{[1-(-1)^j]^2[1-(-1)^k]^2}{jk[j^2+k^2x^2]}\right]^{-1} \tag{2}$$

a dimensionless function which can be written $f \approx 12[1- 0.63\ x^{-1}]^{-1}$ for $1 < x$ (Bruus 2008). We write an estimate of the pressure drop across the front edge of the slug due to the curved two-fluid interface

$$\Delta p_{curv} = \frac{2\gamma}{w}\left(1 + \frac{w}{h}\right). \tag{3}$$

This contribution to the pressure accounts for the presence of curved interfaces in our model. We next consider flat interfaces rather than curved for simplicity's sake. Using these assumptions, we are able to rationalize the breakup dynamics starting at time $t = 0$ when the drop collides with the obstacle. The time at which the rear edge

Fig. 3 Variations of the volume Ω_2 of the daughter drops produced in gap (2) with the velocity of the mother drop v for different viscosities of the dispersed phase: (*circles*) 1, (*squares*) 2.1 and (*diamonds*) 4.1 mPa s. The *lines* are guides for the eyes

of a slug of length L_d meets the obstacle is $t_f = L_d/v$. We next work with the dimensionless time $T = \frac{t}{t_f}$.

Since we work at constant flow rates, a two-fluid interface always invades gap (1) at $t = 0$. Then, it begins to move forward at a speed $d\ell_1/dt$ (see Fig. 4 defining the variables used in our model). A two-fluid interface invades the narrow gap (2) only when the pressure drop Δp between the two ends of the obstacles overcomes the Laplace pressure $\frac{2\gamma}{w_2}\left(1 + \frac{w_2}{h}\right)$ required to accommodate a curved interface in this gap. Prior to the invasion of the narrower gap (2) by a fluid–fluid interface, the position of the interface in the large gap at T, $\ell_1(T) = X_1(T)L$, is obtained by conservation of the total flow rate in Eq. (4): $X_1(T) = \alpha T$ with $\alpha = \frac{L_d w}{L w_1}$. We now consider the situation for which the interface which has entered gap (1) has not yet reached the extremity of the obstacle, that is, $X_1(T) < 1$. Using Eq. (1), we write the pressure drop over L in gap (1), $\Delta p = \frac{\eta_c L q}{h^3 w_1} f_1[(1 + \Delta\eta^s X_1) + \frac{2Z}{C}\left(1 + \frac{w_1}{h}\right)]$, where $\Delta\eta^s = (\eta_d^s - \eta_c)/\eta_c$ and $Z = (f_1 h^{-2} w L)^{-1}$ with

Fig. 4 Top-view schematic of a drop colliding with an obstacle defining the variables used in our model which describes the propagation of two-liquid interfaces in the two gaps

$f_1 = f\left(\frac{w_1}{h}\right)$ are two dimensionless parameters. The condition for the invasion of the narrow gap can be mathematically expressed as $1 + \Delta\eta^s X_1 > \frac{C_\star}{C}$, where $C_\star = 2Z\frac{1-W}{W}$, which provides insights into the importance of the sign of $\Delta\eta^s$. Indeed, when $\Delta\eta^s < 0$, the term on the left-hand side of the inequality, $1 + \Delta\eta^s X_1$, decreases with T, so that the time T_p at which an interface begins to propagate in gap (2) is $T_p = 0$ whenever $C > C_\star$. By contrast, when $\Delta\eta^s > 0$, this term increases with T so that $T_p = \frac{1}{\alpha\Delta\eta^s}\left(\frac{C_\star}{C} - 1\right) \geq 0$. Using the two conditions to be fulfilled to allow propagation in gap (2), $T_p < 1$ and $X_1(T_p) \leq 1$, one finds that invasion occurs when $C > \frac{C_\star}{1+\alpha\Delta\eta^s}$ ($\alpha \leq 1$) or $C > \frac{C_\star}{1+\Delta\eta^s}$ ($\alpha \geq 1$). Note that the extra condition to fulfill, $T_p \geq 0$, gives $T_p = 0$ whenever $C > C_\star$. For both positive and negative $\Delta\eta^s$, if those conditions are not fulfilled when the two-fluid interface exits gap (1), the pressure drop in this gap suddenly decreases and remains constant over time, $\Delta p = \frac{\eta_c L q}{h^3 w_1} f_1[(1 + \Delta\eta^s)$. Then, the pressure drop can no longer become larger that the Laplace pressure mentioned above and the invasion of the narrow gap never occurs.

When $T \geq T_p$, the dynamics of the interfaces present in both gaps are controlled by a set of two coupled first-order ordinary equations whose solutions are X_1 and $X_2 = \ell_2(T)/L$. The conservation of the total flow rate gives

$$\frac{dX_1}{dT} + W\frac{dX_2}{dT} = \alpha. \tag{4}$$

The second one is obtained by the equality of pressure drops over both gaps

$$(1 + \Delta\eta^s X_1)\frac{dX_1}{dT} - FW(1 + \Delta\eta^s X_2)\frac{dX_2}{dT} = \alpha\frac{C_\star}{C} \tag{5}$$

for $X_1 \leq 1$ and $X_2 \leq 1$ and where $W = \frac{w_2}{w_1}$ and $F = f\left(\frac{w_2}{h}\right)/\left[Wf\left(\frac{w_2}{Wh}\right)\right]$.

As we work with a slug size $L_d = 220 \pm 20\,\mu m$ that is constant within experimental errors, we consider that $\alpha = \frac{L_d w}{L w_1} = 0.82 \pm 0.07 < 1$ is constant. Assuming that $\Delta\eta^s > 0$, we now discuss the two cases $C > C_\star$ and $C \leq C_\star$.

- The case $C > C_\star$: We have previously shown that this situation corresponds to $T_p = 0$. By integrating Eqs. (4) and (5) between $T = 0$ and $T = 1$ with the initial conditions $X_1(0) = X_2(0) = 0$, one easily shows that $X_2(1)$ is the positive solution of the quadratic equation

$$X_2(1)^2 W(W - F)\frac{\Delta\eta^s}{2} - X_2(1)W(1 + F + \alpha\Delta\eta^s)$$
$$+ \alpha\left(1 + \frac{\alpha\Delta\eta^s}{2} - \frac{C_\star}{C}\right) = 0. \tag{6}$$

- The case $\mathcal{C} \le \mathcal{C}_{\star}$: We integrate Eqs. (4) and (5) between $T_p = \frac{1}{\alpha \Delta \eta^s} \left(\frac{\mathcal{C}_{\star}}{\mathcal{C}} - 1 \right)$ and $T = 1$ with $X_1(T_p) = \alpha T_p$ and $X_2(T_p) = 0$ as initial conditions. One readily finds that $X_2(1)$ is the positive solution of the following equation

$$X_2(1)^2 W(W - F) \frac{\Delta \eta^s}{2} - X_2(1)W(1 + F + \alpha \Delta \eta^s) + \frac{1}{2\Delta \eta^s}\left(1 + \alpha \Delta \eta^s - \frac{\mathcal{C}_{\star}}{\mathcal{C}}\right)^2 = 0. \tag{7}$$

Since we consider that the slugs have flat interfaces in our modeling work, we estimate $\Omega = L_d wh$ and $\Omega_2 = L_2 w_2 h = X_2(1)Lw_2 h$ so that $X_2(1) = \frac{\alpha \phi_2}{W}$. Using this relationship between $X_2(1)$ and ϕ_2 in Eqs. (6) and (7), one finds that ϕ_2 is the positive solution of the quadratic equation

$$\phi_2^2 \frac{(F - W)\zeta}{2W} + \phi_2(1 + F + \zeta) - A(\zeta, \mathcal{C}, \mathcal{C}_{\star}) = 0 \tag{8}$$

with $\zeta = \alpha \Delta \eta^s$ and where

- $A(\zeta, \mathcal{C}, \mathcal{C}_{\star}) = 1 + \frac{\zeta}{2} - \frac{\mathcal{C}_{\star}}{\mathcal{C}}$ when $\mathcal{C} > \mathcal{C}_{\star}$;

- $A(\zeta, \mathcal{C}, \mathcal{C}_{\star}) = \frac{1}{2\zeta}\left(1 + \zeta - \frac{\mathcal{C}_{\star}}{\mathcal{C}}\right)^2$ when $\mathcal{C} \le \mathcal{C}_{\star}$.

One then easily shows that

$$\phi_2 = \frac{W(1 + F + \zeta)}{(F - W)\zeta}\left(-1 + \sqrt{1 + \frac{2A(F - W)\zeta}{W(1 + F + \zeta)^2}}\right). \tag{9}$$

As discussed above, the outcome of our model is Eq. (9) that gives an analytical expression for the variations of ϕ_2 with $\mathcal{C}$ and other dimensionless parameters describing the geometry; finding an expression of ϕ_1 is then immediate as $\phi_1 = 1 - \phi_2$. As shown in Fig. 5, the theoretical prediction provided by Eq. (9) describes remarkably well our experimental data considering there is only one free parameter, ζ, in the model (Fig. 6).

For the discussed case $\Delta \eta^s > 0$ and $\alpha < 1$, Salkin et al. (2012) have shown that breakup occurs whenever an interface enters the narrow gap. In other words, the threshold $\mathcal{C}_b$ corresponds to the capillary number $\frac{\mathcal{C}_{\star}}{1+\zeta}$ above which an interface propagates in the gap (2). In Fig. 6, we report the variations of $\mathcal{C}_b = \frac{\mathcal{C}_{\star}}{1+\zeta}$ with p determined by using the best fits to our data shown in Fig. 5. Figure 6 shows that that $\mathcal{C}_b$ takes values that are surprisingly much smaller ($\propto 10^{-3}$) than those required to break a drop under shear flow in bulk ($\propto 1$). We also note that in our microfluidic experiments, $\mathcal{C}_b$ is a decreasing function of p in the investigated range [0.2–2].

In Fig. 7, we report the values found for the free parameter ζ as a function of p. Since $\alpha = 0.82 \pm 0.07$
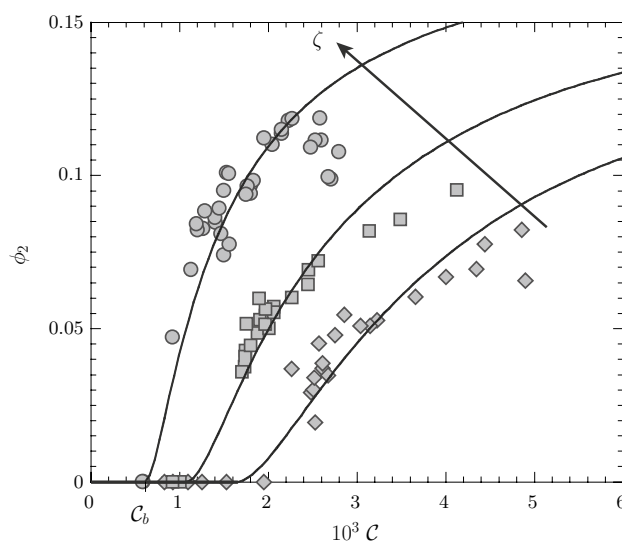

Fig. 5 Variations of the volume fraction ϕ_2 of the daughter drops formed in gap (2) with the capillary number $\mathcal{C}$ for different aqueous solutions; the *symbols* are identical to those in Fig. 3. The *lines* correspond to the prediction of ϕ_2 given by Eq. (9) with the following values of the free parameter $\zeta = \alpha \Delta \eta^s$: (*circles*) 2.04, (*squares*) 3.68 and (*diamonds*) 7.35
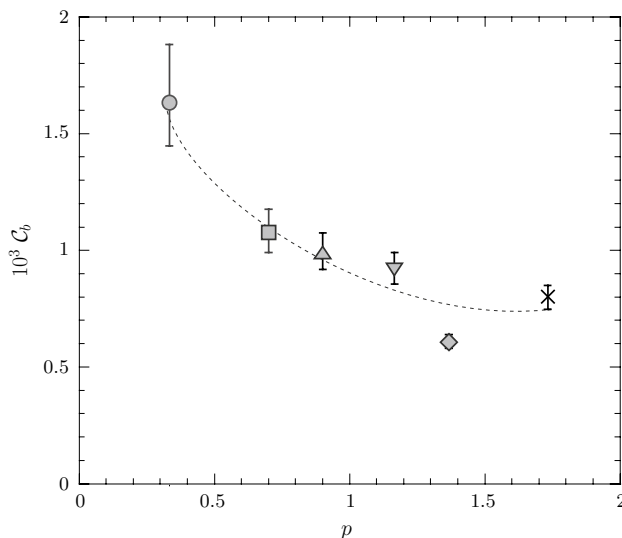
Fig. 6 Evolution of $\mathcal{C}_b$ with the viscosity ratio p. The *symbols* stand for different viscosities of the dispersed phase: (*up-pointing triangles*) 2.7, (*down-pointing triangles*) 3.5 and (*times sign*) 5.2 mPa s and as indicated in Table 1. The *line* is a guide for the eyes

is constant within experimental errors in our study, our analysis allows us to estimate the free parameter $\Delta \eta^s$ characterizing the effective viscosity introduced by the flow of slugs. We find that $\Delta \eta^s = 2.5 - 6.5 > 0$ for our experiments which validates the assumption made when modeling ϕ_2. We also note that $\Delta \eta^s$, thus η_d^s, increases
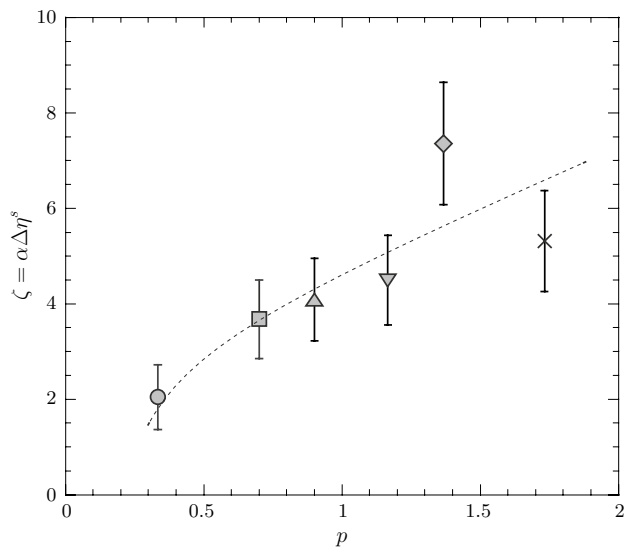
Fig. 7 Variations of ζ with p. The *symbols* are identical to those of figure and the *line* is a guide of the eyes

with p (Fig. 7). The values we found for this system for $\eta_d^s = (1 + \Delta\eta^s)\eta_c = 10.5$–$22.5$ are larger than η_c in agreement with previous results by Salkin et al. (2012) also conducted with an aqueous solution in oil system.

5 Conclusion

We have studied the breakup of drops flowing against a rectangular obstacle placed off-center in a microchannel. In agreement with earlier works, we have shown that breakup requires that the capillary number $\mathcal{C}$ exceeds a threshold $\mathcal{C}_b$. We have characterized the role of the viscosity ratio p between dispersed and continuous phases on drop breakup by investigating the experimental variations of the volume fraction ϕ_2 of the smaller daughter droplet formed upon breakup of a mother drop with $\mathcal{C}$ and p. We have presented a single free parameter model that gives an analytical expression of ϕ_2 which captures these variations and allows us to determine $\mathcal{C}_b$. We find a threshold for breakup that is three orders of magnitude smaller than typical values found under shear flow in bulk experiments. In addition, our results show that $\mathcal{C}_b$ is decreasing with p in the that studied range of the viscosity ratio [0.2–2].

References

Abate AR, Weitz DA (2011) Faster multiple emulsification with drop splitting. Lab Chip 11(11):1911–1915

Afkhami S, Leshansky AM, Renardy Y (2011) Numerical investigation of elongated drops in a microfluidic T-junction. Phys Fluids 23(2):022002

Anna SL, Bontoux N, Stone HA (2003) Formation of dispersions using flow focusing. Appl Phys Lett 82(3):364–366

Baroud CN, de Saint R, Vincent M, Delville JP (2007) An optical toolbox for total control of droplet microfluidics. Lab Chip 7(8):1029–1033

Bedram A, Moosavi A (2011) Droplet breakup in an asymmetric microfluidic T junction. Eur Phys J E 34(8):78

Bedram A, Moosavi A, Hannani SK (2015) Analytical relations for long-droplet breakup in asymmetric T junctions. Phys Rev E 91(5):053012

Belloul M, Courbin L, Panizza P (2011) Droplet traffic regulated by collisions in microfluidic networks. Soft Matter 7(9):9453–9458

Bentley B, Leal L (1986) An experimental investigation of drop deformation and breakup in steady, two-dimensional linear flows. J Fluid Mech 167:241283

Bruus H (2008) Theoretical microfluidics. Oxford University Press, New-York

Cardinaels R, Moldanaers P (2011) Critical conditions and breakup of non-squashed microconfined droplets: effects of fluid viscoelasticity. Microfluid Nanofluid 10(6):1153–1163

Che ZZ, Nguyen NT, Wong TN (2011) Hydrodynamically mediated breakup of droplets in microchannels. Appl Phys Lett 98(5):054102

Chu LY, Utada AS, Shah RK, Kim JW, Weitz DA (2007) Controllable monodispersed multiple emulsions. Angew Chem Int Ed 46(47):8970–8974

Chung C, Lee M, Chan K, Ahn KH, Lee SJ (2010) Droplet dynamics passing though obstructions in confined microchannel flow. Microfluid Nanofluid 9(6):1151–1163

Courbin L, Panizza P, Salmon JB (2004a) Observations of droplet size oscillations in a two phase fluid under shear flow. Phys Rev Lett 92(1):018305

Courbin L, Engl W, Panizza P (2004b) Can a droplet break up under flow without elongating? Fragmentation of smectic monodisperse droplets. Phys Rev E 69(6):061508

Cubaud T (2009) Deformation and breakup of high-viscosity droplets with symmetric microfluidic cross flows. Phys Rev E 80(2):026307

de Menech M (2006) Modeling of droplet breakup in a microfluidic T-shaped junction with a phase-field model. Phys Rev E 73(3):031505

Engl W, Backov R, Panizza P (2008) Controlled production of emulsions and particles by milli- and microfluidic techniques. Curr Opin Colloid Interface Sci 13(4):206216

Grace HP (1982) Dispersion phenomena in high viscosity immiscible fluid systems and application of static mixer as dispersion devices in such systems. Chem Eng Commun 14:225–277

Guido S (2011) Shear-induced droplet deformation: effects of confined geometry and viscoelasticity. Curr Opin Colloid Interface Sci 16(1):61–70

Gupta A, Sbragaglia M (2014) Deformation and breakup of viscoelastic droplets in confined shear flow. Phys Rev E 90(2):023305

Huere A, Theodoly O, Leshansky AM, Valignat MP, Cantat I, Jullien MC (2015) Droplets in microchannels: dynamical properties of the lubrication film. Phys Rev Lett 115(6):064501

Janssen JMH, Meijer HEM (1993) Droplet breakup mechanisms. J Rheol 37(4):597608

Leal-Calderon F, Schmitt V, Bibette J (2007) Emulsion science: basic principles, 2nd edn. Springer, New York

Leshansky AM, Pismen LM (2009) Breakup of drops in a microfluidic T junction. Phys Fluids 21(2):023303

Li QX, Chai ZH, Shi BC, Liang H (2014) Deformation and breakup of a liquid droplet past a solid circular cylinder: a lattice Boltzmann study. Phys Rev E 90(4):043015

Link DR, Anna SL, Weitz DA, Stone HA (2004) Geometrically mediated breakup of drops in microfluidic devices. Phys Rev Lett 92(5):054503

Link DR, Grasland-Mongrain E, Duri A, Sarrazin F, Cheng Z, Cristobal G, Marquez M, Weitz DA (2006) Electric control of droplets in microfluidic devices. Angew Chem Int Ed 45(16):2556–2560

McDonald JC, Duffy DC, Anderson JR, Chiu DT, Wu H, Schueller OJ, Whitesides GM (2000) Fabrication of microfluidic systems in poly(dimethylsiloxane). Electrophoresis 21(1):27–40

Ménétrier-Deremble L, Tabeling P (2006) Droplet breakup in microfluidic junctions of arbitrary angles. Phys Rev E 74(3):035303R

Mighri F, Carreau PJ, Ajji A (1998) Influence of elastic properties on drop deformation and breakup in shear flow. J Rheol 42(6):1477–1490

Prat L, Sarrazin F, Tasseli J, Marty A (2006) Increasing and decreasing droplets velocity in microchannels. Microfluid Nanofluid 2(3):271–274

Protière S, Bazant MZ, Weitz DA, Stone HA (2010) Droplet breakup in flow past an obstacle: a capillary instability due to permeability variations. Europhys Lett 92(5):54002

Rayleigh L (1878) On the instability of jets. Proc London Math Soc 10:4

Salkin L, Courbin L, Panizza P (2012) Microfluidic breakups of confined droplets against a linear obstacle: the importance of the viscosity contrast. Phys Rev E 86(3):036317

Salkin L, Schmit A, Courbin L, Panizza P (2013) Passive breakups of isolated drops and one-dimensional assemblies of drops in microfluidic geometries: experiments and models. Lab Chip 13(15):3022–3032

Samie M, Salari A, Shafii MB (2013) Breakup of microdroplets in asymmetric T junctions. Phys Rev E 87(5):053003

Schmit A, Salkin L, Courbin L, Panizza P (2015) Cooperative breakups induced by drop-to-drop interactions in one-dimensional flows of drops against micro-obstacles. Soft Matter 11(4):2454–2460

Seeman R, Brinkmann M, Pfohl T, Herminghaus S (2012) Droplet based microfluidics. Rep Prog Phys 75(1):016601

Sessoms DA, Amon A, Courbin L, Panizza P (2010) Complex dynamics of droplet traffic in a bifurcating microfluidic channel: periodicity, multistability, and selection rules. Phys Rev Lett 105(15):154501

Shah RK, Shum HC, Rowat AC, Lee D, Agresti JJ, Utada AS, Chu LY, Kim JW, Fernandez-Nieves A, Martinez J, Weitz DA (2008) Designer emulsions using microfluidics. Mater Today 11(4):18–27

Stone HA (1994) Dynamics of drop deformation and breakup in viscous fluids. Annu Rev Fluid Mech 26:65102

Stone HA, Leal LG (1989) Relaxation and breakup of an initially extended drop in an otherwise quiescent fluid. J Fluid Mech 198:399427

Tan J, Xu JH, Li SW, Luo GS (2008) Drop dispenser in a cross-junction microfluidic device: scaling and mechanism of break-up. Chem Eng J 136(2–3):306–311

Taylor GI (1932) The viscosity of a fluid containing small drops of another fluid. Proc R Soc Lond A 138:41–48

Taylor GI (1934) The formation of emulsions in definable fields of flow. Proc R Soc Lond A 146:501–523

Teh SY, Lin R, Hung LH, Lee AP (2008) Droplet microfluidics. Lab Chip 8(2):198–220

Torza S, Cox RG, Mason SG (1972) Particle motions in sheared suspensions XXVII. Transient and steady deformation and burst of liquid drops. J Colloid Interface Sci 38:395–411

Trivedi V, Doshi A, Kurup GK, Ereifej E, Vandevord PJ, Basu AS (2010) A modular approach for the generation, storage, mixing, and detection of droplet libraries for high throughput screening. Lab Chip 10(18):2433–2442

Vananroye A, Van Puyvelde P, Moldanaers P (2006) Effect of confinement on droplet breakup in sheared emulsions. Langmuir 22(9):3972–3974

Vananroye A, Van Puyvelde P, Moldanaers P (2007) Effect of confinement on the steady-state behavior of single droplets during shear flow. J Rheol 51(1):139–153

Wang J, Yu D (2015) Asymmetry of flow fields and asymmetric breakup of a droplet. Microfluid Nanofluid 18(4):709715

Zheng MM, Ma YL, Jin TM, Wang JT (2016) Effects of topological changes in microchannel geometries on the asymmetric breakup of a droplet. Microfluid Nanofluid 20(7):107